Frontiers in Bioscience Landmark

Front. Biosci. (Landmark Ed) **2026**; 31(8): 52801
https://doi.org/10.31083/FBL52801

Original Research

IFIT1$^+$ Tumor-Associated Macrophages Suppress Cancer Stemness and Enhance Chemosensitivity via the TNFSF10–TNFRSF10B Axis in Epithelial Ovarian Cancer

Rui Liu[1,2,3,4], Yilin Fang[2,3,4], Ruxi Zheng[2,3,4], Liya Lin[5], Da Huang[1,2,3,4], Lingyun Zhai[2,3,4], Qionghua He[2,3,4], Zhigang Zhang[2,3,4], Jianwei Zhou[2,3,4,*], Xiaoming Zhang[2,6,*]

[1]Department of Basic Medicine Sciences, The Second Affiliated Hospital, School of Medicine, Zhejiang University, 310009 Hangzhou, Zhejiang, China
[2]Department of Gynecology, The Second Affiliated Hospital, School of Medicine, Zhejiang University, 310009 Hangzhou, Zhejiang, China
[3]Zhejiang Provincial Clinical Research Center for Gynecological Diseases, 310006 Hangzhou, Zhejiang, China
[4]Key Laboratory of Cancer Invasion and Metastasis (HUST), Ministry of Education, 430100 Wuhan, Hubei, China
[5]Clinical Research Center, The Second Affiliated Hospital, School of Medicine, Zhejiang University, 310009 Hangzhou, Zhejiang, China
[6]School of Basic Medical Sciences, Zhejiang University, 310058 Hangzhou, Zhejiang, China
*Correspondence: 2195045@zju.edu.cn (Jianwei Zhou); zxm@zju.edu.cn (Xiaoming Zhang)
Academic Editor: Jordi Sastre-Serra
Submitted: 10 April 2026 Revised: 19 June 2026 Accepted: 25 June 2026 Published: 31 July 2026

Abstract

Background: Epithelial ovarian cancer (EOC) is typically diagnosed at an advanced stage and is associated with high mortality due to metastasis and chemoresistance. Cancer stem cells (CSCs) are central to EOC progression, recurrence, and treatment resistance, with their functional behavior shaped by the tumor immune microenvironment. While M1 and M2 macrophages have been well-characterized, the role of interferon-stimulated gene-enriched subpopulations, particularly interferon-induced protein with tetratricopeptide repeats 1 tumor-associated macrophages (IFIT1$^+$ TAMs), in regulating CSC properties in EOC remains largely unexplored. **Methods:** Single-cell RNA sequencing (scRNA-seq) was utilized to map the myeloid landscape and trace transcriptomic evolution in EOC. An *in vitro* indirect culture model utilizing unpolarized macrophage (M0)-conditioned medium (CM) was established to assess baseline phenotypic alterations. Furthermore, targeted siRNA silencing (si-*TNFRSF10B*) combined with recombinant human tumor necrosis factor ligand superfamily member 10 (TNFSF10) (rhTRAIL) treatments were employed to evaluate the specific impact of the TNF-related apoptosis-inducing ligand (TRAIL)-Death receptor 5 (DR5) signaling axis on multidrug resistance and CD44 expression. **Results:** High-resolution scRNA-seq analysis revealed a stage-dependent decline in IFIT1$^+$ TAMs, an interferon-primed subset that robustly expresses the TNFSF10 ligand during early-stage disease. *In vitro* assays showed that conditioned medium from M0 macrophages suppresses CSC features and enhances expression of the tumor necrosis factor receptor superfamily member 10B (Death receptor 5) (TNFRSF10B/DR5) in EOC cells. Mechanistic studies confirmed that exogenous rhTRAIL treatment markedly diminished CD44$^+$ cell populations and enhanced sensitivity to chemotherapeutic agents. Notably, these antitumor effects were largely abrogated following siRNA-mediated silencing of the DR5 receptor in EOC cell lines. **Conclusions:** Our findings reveal that IFIT1$^+$ tumor-associated macrophages intrinsically harbor anti-cancer stem cell potential through the TNFSF10 ligand. Activation of the TNFSF10-TNFRSF10B pathway suppresses cancer stemness and may enhance chemosensitivity. These insights shed light on the functional diversity of macrophages, highlighting that driving tumor-associated macrophages toward a sustained, interferon-primed IFIT1$^+$ phenotype represents a promising therapeutic approach to target cancer stem cell populations in epithelial ovarian cancer.

Keywords: epithelial ovarian cancer; cancer stem cells; IFIT1$^+$ tumor-associated macrophages; tumor microenvironment; single-cell RNA sequencing

1. Background

Epithelial ovarian cancer (EOC) ranks among the most prevalent and deadly gynecological cancers, contributing substantially to cancer-related mortality in women globally [1]. Although surgical and chemotherapeutic strategies have advanced, the prognosis for EOC patients remains dismal, largely owing to frequent tumor recurrence and acquired chemoresistance [2]. Cancer stem cells (CSCs), a distinct subset of tumor cells endowed with self-renewal and multilineage differentiation potential, are widely regarded as central orchestrators of tumor initiation, progression, and therapeutic resistance [3]. The stem-like attributes of CSCs underlie the pronounced heterogeneity and aggressive behavior of EOC, presenting a formidable barrier to effective therapeutic intervention [4]. Therefore, understanding the mechanisms that regulate CSC behavior has emerged as a critical area of research in EOC therapy [5].

The tumor microenvironment (TME) exerts a decisive influence on shaping cancer stem cell traits and driving tu-

Copyright: © 2026 The Author(s). Published by IMR Press.
This is an open access article under the CC BY 4.0 license.

Publisher's Note: IMR Press stays neutral with regard to jurisdictional claims in published maps and institutional affiliations.

mor evolution [6]. Among the various immune cells in the TME, macrophages are particularly influential due to their plasticity and diverse functional states [7]. Traditionally, macrophages in the TME have been categorized into the classically activated M1 phenotype and the alternatively activated M2 phenotype [8]. However, this simplistic binary paradigm is increasingly recognized as insufficient to capture the full spectrum of macrophage plasticity and functional heterogeneity *in vivo*. Recent pan-cancer single-cell transcriptomic analyses have identified conserved intermediate or interferon-responsive states, notably the IFIT1$^+$ tumor-associated macrophages (TAMs), which are characterized by the robust expression of interferon-stimulated genes (ISGs) [9,10]. While the roles of M1 and M2 macrophages in cancer progression have been extensively studied, the functions of these IFIT1$^+$ TAMs continue to be poorly understood [11]. This knowledge gap limits our understanding of how macrophage heterogeneity influences EOC stemness and clinical outcomes, ultimately hindering our ability to develop targeted therapies and improve patient prognoses.

The primary objective of this study is to elucidate the relationship between different macrophage functional states and CSCs in EOC by combining bioinformatics analysis with clinical data from The Cancer Genome Atlas (TCGA) database [12] and *in vitro* experiments. Specifically, by analyzing treatment-naive EOC cohorts to preserve the unperturbed tumor immune landscape, we aim to explore how IFIT1$^+$ TAMs regulate the stem cell characteristics and chemoresistance of EOC to influence tumor progression. After initially observing the distinct effects of general macrophage polarization states on CSCs *in vitro*, we utilized single-cell RNA sequencing to identify the specific TAM subpopulation driving these phenotypes. Through comprehensive ligand-receptor validation and molecular rescue experiments utilizing siRNA-mediated tumor necrosis factor receptor superfamily member 10B (Death receptor 5) (*TNFRSF10B*/DR5) knockdown alongside exogenous tumor necrosis factor ligand superfamily member 10 (TNFSF10) protein, we seek to uncover novel signaling pathways and molecular mechanisms underlying macrophage-CSC interactions, which would provide new insights into EOC biology and more effective therapeutic targets.

2. Methods

2.1 Data Collection

RNA sequencing data and associated clinical metadata for EOC were obtained from TCGA database (accessible at https://portal.gdc.cancer.gov). Raw counts in Spliced Transcripts Alignment to a Reference (STAR)-counts format were transformed into transcripts per million (TPM) and further normalized via the $\log_2$(TPM + 1) transformation. After integrating transcriptomic profiles with clinical annotations, a final cohort of 374 samples fulfilling all eligibility criteria was selected for downstream analyses. For the TCGA cohort, the inclusion criteria were strictly defined as follows: (i) histologically confirmed primary high-grade serous ovarian cancer (HGSOC); (ii) availability of complete bulk transcriptomic profiling (RNA-seq) data; and (iii) documented pathological staging alongside longitudinal clinical follow-up records. Patients with non-serous histological subtypes or incomplete clinical annotation were excluded. Notably, among the 374 cases included in the survival cohort, 1 case lacked explicit pathological stage information and was therefore omitted from stage-specific comparisons (n = 373).

Clinical data and single-cell RNA sequencing (scRNA-seq) data were acquired from the Gene Expression Omnibus (GEO) (GSE184880: n = 7; GSE201047: n = 3) [13,14]. To preserve the intact tumor immune microenvironment, these ten cases (7 early-stage, 3 late-stage) were stringently selected based on their treatment-naive status—defined as no prior administration of neoadjuvant chemotherapy or immunotherapy. Notably, all scRNA-seq datasets were generated solely from primary tumor tissues, with no inclusion of normal or benign ovarian samples, consistent with our focused investigation of intratumoral microenvironmental dynamics.

2.2 Single Cell RNA Data Processing and Analysis

Stringent initial quality control was applied to the single-cell data by retaining only cells expressing over 200 genes and filtering out those with mitochondrial UMI ratios surpassing 20%. Mitochondrial genes were then excluded from downstream analysis by removal from the expression matrix. Data normalization and scaling were conducted using the Seurat package (version 4.1.1, available at https://satijalab.org/seurat/). This step effectively corrected for confounding factors such as sequencing depth and mitochondrial contamination. To address technical heterogeneity stemming from distinct study sources and sequencing platforms in the two GEO cohorts, raw expression matrices were integrated and rigorously corrected for batch effects using the Harmony algorithm. Both individual patient identifiers and dataset sources were designated as batch covariates to ensure effective harmonization. Principal component analysis (PCA) was applied to the scaled data, utilizing the top 2000 highly variable genes, and the first 10 principal components were selected for dimensionality reduction via Uniform Manifold Approximation and Projection (UMAP). Cell clusters were delineated via a graph-based clustering approach built upon the first 10 principal components. Marker genes for each cluster were determined using the FindAllMarkers function, employing the Wilcoxon rank-sum test with the following thresholds: |log2 fold change| >0.25, adjusted p-value < 0.05, and minimum percentage of cells expressing the gene >10%. For refined cell type annotation, clusters preliminarily assigned to the same

lineage underwent iterative re-clustering and marker gene assessment using an identical analytical workflow.

2.3 Pathway Analysis

To explore the biological functions and signaling pathways linked to differentially expressed genes (DEGs) and cluster-defining markers, pathway enrichment analysis was carried out using the Kyoto Encyclopedia of Genes and Genomes (KEGG) database. Statistical significance of the enriched pathways was assessed using Fisher's exact test as the underlying statistical engine to calculate the probability of gene overlap. To account for multiple testing and reduce false discoveries, significance was determined using a false discovery rate (FDR) correction (Benjamini-Hochberg method) with an adjusted **p**-value threshold of <0.05.

2.4 Pseudotime Analysis

To reconstruct the developmental trajectories of cell populations, single-cell pseudotime analysis was conducted using Monocle2 (available at http://cole-trapnell-lab.github.io/monocle-release). The DDR-Tree algorithm was employed with default parameters to model the branching dynamics and state transitions among cell types and clusters. Input for trajectory inference included both Seurat-derived marker genes and the raw expression matrix from quality-controlled cells. Furthermore, Branch Expression Analysis Modeling (BEAM) was utilized to detect genes exhibiting differential expression patterns at key branch points, thereby highlighting candidates involved in cell fate specification during pseudotemporal progression.

2.5 Cell–Cell Communication Analysis

To systematically explore intercellular signaling networks, we conducted cell-cell communication analysis using CellPhoneDB (version 1.1.0, Hinxton, Cambridgeshire, UK), a curated repository of ligand-receptor pairs and their potential interactions. Membrane-bound, secreted, and peripheral proteins were annotated for each cell cluster. The statistical significance of inferred cellular communication events was assessed by computing interaction scores and adjusted *p*-values ($p < 0.05$), derived from the normalized gene expression matrix produced by Seurat's preprocessing workflow.

2.6 Inferring Tumor-Infiltrating Immune Cell Abundance

The immune cell composition in the TCGA dataset was analyzed using the Cell-type Identification by Estimating Relative Subsets of RNA Transcripts (CIBERSORT) tool (https://cibersort.stanford.edu/), employing the LM22 signature matrix as a reference to estimate the proportions of various immune cell types.

2.7 Immunohistochemical Staining and Analysis

A total of 20 EOC patients who underwent primary surgical resection at the Second Affiliated Hospital of Zhejiang University between 2020 and 2023 were enrolled in this study. This is a retrospective clinical study using archived formalin-fixed paraffin-embedded (FFPE) tumor tissues from 2020 to 2023. This study was conducted in accordance with the Declaration of Helsinki and approved by the Institutional Ethics Committee of the Second Affiliated Hospital of Zhejiang University (Approval No. 2025-0642). All patients were treatment-naïve and had not received any neoadjuvant therapy before surgery. Immunohistochemistry (IHC) staining and analysis were conducted on 3 μm sections obtained from 20 patients, which were processed by Biossci Biotechnology Co., Ltd. Following a series of steps including deparaffinization, antigen unmasking, and blocking, the slides were incubated overnight at 4 °C with a rabbit-derived anti-CD44 antibody (Cat No. ab189524, Abcam, Cambridge, UK) at a dilution of 1:16,000 and rabbit-derived anti-IFIT1 antibody (Cat No. 83423-1-RR, Proteintech, Wuhan, Hubei, China) at a dilution of 1:200. Sections were then developed with 3,3'-Diaminobenzidine (DAB) chromogen and counterstained with hematoxylin. A semi-automated quantitative method was used to assess IFIT1 and CD44 immunoreactivity. To minimize false-positive signals from irrelevant cell populations, two independent, board-certified pathologists manually defined regions of interest (ROIs) on each slide. For $IFIT1^{+}$ tumor-associated macrophages (TAMs), only stromal areas enriched with morphologically identifiable macrophages were selected, with strict exclusion of epithelial tumor nests. In contrast, compact tumor nests were designated as ROIs for evaluating CD44-positive CSCs. To ensure consistency in assessing positive staining across all images, immunohistochemical quantification was performed using the "Split channels" function (blue channel) from Fiji-ImageJ® software (version 1.54p, National Institutes of Health, Bethesda, MD, USA). The percentage of positive area (% positive area) was calculated as the ratio of thresholded positive pixels within the pathologist-defined ROIs to the total ROI area.

2.8 Cell Culture and Preparation of CM

HEY and SKOV3 cells were purchased from Procell (Cat No. CL-0671 and Cat No. CL-0215, Procell, Wuhan, Hubei, China). A2780 cells were purchased from the Cell Bank of the Chinese Academy of Sciences (Cat No. SCSP-5477S, CAS Cell Bank, Shanghai, China). THP-1 cells were purchased from Meilun BioTech (Cat No. PWE-HU003, Meilun BioTech, Dalian, Liaoning, China). All cell lines were maintained at 37 °C in a humidified 5% CO2 atmosphere and were mycoplasma-free (MycoBlue Mycoplasma Detector, Cat No. D101-01, Vazyme, Nanjing, China). All cell lines were authenticated shortly before

use by short tandem repeat (STR) profiling, carried out by Procell (Procell, Wuhan, Hubei, China).

HEY and SKOV3 cells were cultured in Dulbecco's Modified Eagle Medium (DMEM) (Cat No. 319-005-CL, Wisent, Saint-Jean-Baptiste, Quebec, Canada) with 10% fetal bovine serum (FBS) (Cat No. C04001, XP Biomed, Shanghai, China) and 1% penicillin/streptomycin (Cat No. PS2004HY, TBSscience, Tianjin, China). A2780 and THP-1 cells were cultured in RPMI 1640 (Cat No. 350000120, Wisent, Saint-Jean-Baptiste, Quebec, Canada) with 10% FBS and 1% penicillin/streptomycin, and β-mercaptoethanol (0.05 mM, Cat No. M6230, Macklin, Shanghai, China) was supplemented to the THP-1 culture medium. THP-1 monocytes were treated with 100 ng/mL phorbol 12-myristate 13-acetate (PMA, Cat No. P8139, Sigma-Aldrich, St. Louis, MO, USA) in complete culture medium for 48 h to induce differentiation. The suspension-grown THP-1 monocytes differentiated into adherent M0 macrophages exhibiting extended cellular protrusions. In THP-M0, M1 macrophages (THP-M1) were induced with interferon-gamma (IFN-γ) (20 ng/mL, Cat No. PCK062, Procell, Wuhan, Hubei, China) and lipopolysaccharide (LPS) (100 ng/mL, Cat No. A1228298, Ambeed, Shanghai, China) for 48 h while M2 macrophages (THP-M2) were induced with IL-13 (20 ng/mL, Cat No. PCK174, Procell, Wuhan, Hubei, China) and IL-4 (20 ng/mL, Cat No. PCK032, Procell, Wuhan, Hubei, China) for 48 h [15]. Macrophage polarization efficiency was confirmed by flow cytometry. The gating strategy is shown in **Supplementary Fig. 3**. Thereafter, M0, M1, and M2 macrophages were cultured in serum-free RPMI 1640 medium for an additional 72 h to collect conditioned medium (CM). The collected CM was added to the culture system by 30% for subsequent co-culture with cancer cell lines. For mechanistic validation, EOC cells were treated with recombinant human TNFSF10 (rhTRAIL, Cat No. C022, Novoprotein, Shanghai, China) at a concentration of 100 ng/mL for 24 h.

2.9 siRNA Knockdown

EOC cells were seeded in culture plates and transfected at 60–80% confluence. For targeted gene silencing, specific si-*TNFRSF10B* and scrambled negative control siRNA (si-NC) (GenePharma, Shanghai, China) were transfected using siRNA-Mate plus reagent (G04026, GenePharma, Shanghai, China) according to the manufacturer's instructions. Briefly, siRNAs and the transfection reagent were diluted and mixed in a serum-free medium to form complexes, followed by addition to the cells at a final amount of 15 pmol per well (24-well format). After 4–6 h of incubation, the transfection mixture was replaced with a fresh complete medium. Cells were harvested 48–72 h later for downstream analyses. All experiments included scrambled si-NC, reagent-only, and untreated control groups. All experiments were performed with at least three independent biological replicates.

The specific siRNA sequences targeting *TNFRSF10B* were designed and synthesized by GenePharma (Shanghai, China). The sequences are as follows:

TNFRSF10B siRNA-1 sense: 5′-GUGGCUGUGUUUGUUUGCATT-3′

TNFRSF10B siRNA-1 antisense: 5′-UGCAAACAAACACAGCCACTT-3′

2.10 Cell Survival Assay

Carboplatin, docetaxel, and doxorubicin (Cat No. MB1297-1, MB1081-1, MB1087-1; Meilun, Dalian, Liaoning, China) were serially diluted using 0.9% saline solution to achieve a range of desired concentrations. SKOV3, A2780, and HEY cells were seeded into 96-well plates at a density of 5000 cells per well. Following cell adherence, both the THP-CM-treated and control groups were exposed to varying concentrations of carboplatin, docetaxel, or doxorubicin. Cell Counting Kit-8 (CCK-8) assay kit (Cat No. KGA9306-500, Jiangsu KeyGEN BioTECH, Nanjing, Jiangsu, China) was used to assess the cell viability following a 48 h treatment. OD450 was read on a multifunctional microplate reader. There were three duplicate wells in each group.

2.11 Flow Cytometry Analysis for CSCs

Cells from both treatment and control groups were incubated with APC-conjugated anti-CD44 antibody (Cat No. 338805, BioLegend, San Diego, CA, USA) for 20 minutes at 4 °C to evaluate CD44 expression, a surface marker associated with CSCs. After resuspension in phosphate-buffered saline (PBS), the labeled cells were analyzed by flow cytometry using a BD LSRFortessa™ Cell Analyzer (Cat No. 647794, BD Biosciences, San Jose, CA, USA).

2.12 RNA Extraction and Quantitative Real-Time PCR

Total RNA from cancer cell lines and cultured macrophages was isolated using the Quick RNA Extraction Kit (Cat No. AG21023, Accurate Biotech, Changsha, Hunan, China), following the manufacturer's protocol. RNA concentrations were assessed using a NanoDrop spectrophotometer (Thermo Fisher Scientific, Waltham, MA, USA). cDNA synthesis was performed with the Evo M-MLV RT Premix (Cat No. AG11706, Accurate Biotech, Changsha, Hunan, China). Quantitative real-time PCR (qRT-PCR) was conducted on the CFX96 Touch Real-Time PCR System (Cat No. 1855196, Bio-Rad, Hercules, CA, USA) using the SYBR® Green Premix Pro Taq HS qPCR Kit (Cat No. AG11701, Accurate Biotech, Changsha, Hunan, China). To ensure accurate quantification, Glyceraldehyde-3-phosphate dehydrogenase (*GAPDH)* served as an endogenous reference for normalizing RNA expression levels. Each sample was analyzed in triplicate, and the mean ± standard error was calculated for each data point.

The primer sequences were as follows:

HEBP1 Forward: 5′-GACAGATAAGCCTGTGGATGAGG-3′

HEBP1 Reverse: 5′-GCAGAGAGCCATCTTCATTGGG-3′;

RORA Forward: 5′-ACTCCTGTCCTCGTCAGAAGA-3′

RORA Reverse: 5′-CATCCCTACGGCAAGGCATTT-3′;

TNFRSF10B Forward: 5′-AGCACTCACTGGAATGACCTCC-3′

TNFRSF10B Reverse: 5′-GTGCCTTCTTCGCACTGACACA-3′

GAPDH Forward: 5′-TTCAATGGCACAGTCAAGGC-3′

GAPDH Reverse: 5′-TCACCCCATTTGATGTTAGCG-3′.

2.13 Western Blot Analysis

Western blotting was carried out according to the manufacturer's protocols. Briefly, cells were lysed on ice using Radioimmunoprecipitation assay (RIPA) lysis buffer (Cat No. PS0012, Leagene Biotechnology, Beijing, China). The total protein concentration was determined using a bicinchoninic acid (BCA) Protein Assay Kit (Cat No. P0012, Beyotime Biotechnology, Shanghai, China) according to the manufacturer's instructions. A standard curve was generated using bovine serum albumin (BSA; ST023, Beyotime Biotechnology, Shanghai, China), and absorbance was read at 590 nm on a visible spectrophotometer to determine sample protein concentrations. Extracted proteins were collected, denatured, and separated via 10% sodium dodecyl sulfate-polyacrylamide gel electrophoresis (SDS-PAGE). Electrophoresis was run for 60–90 minutes after sample loading. The resolved proteins were then transferred to a nitrocellulose (NC) membrane, which was blocked with 5% BSA at 37 °C. Following blocking, the membrane was agitated on a shaker for 2 h.

After 2 h of shaking, the membrane was washed. The membranes were then incubated with primary antibodies: HEBP1 (1:2000, Cat No. 82950-1-RR, Proteintech, Wuhan, Hubei, China), RORA (1:500, Cat No. A6971, Abclonal Technology, Woburn, MA, USA), TNFRSF10B (1:500, Cat No. A21912, ABclonal Technology, Woburn, MA, USA), GAPDH (1:5000, Cat No. EM1101, HUABIO, Hangzhou, Zhejiang, China), and β-actin (1:5000, Cat No. HA722023, HUABIO, Hangzhou, Zhejiang, China). The membranes were then incubated in secondary antibodies (Horseradish peroxidase (HRP) conjugated goat anti-rabbit IgG polyclonal antibody, 1:5000 dilution, Cat No. HA1001; and HRP-conjugated goat anti-mouse IgG polyclonal antibody, 1:5000 dilution, Cat. No. HA1006; HUABIO, Hangzhou, Zhejiang, China) at room temperature for 2 h and washed in Tris-buffered saline with Tween 20 (TBST) three times for 15 min. Protein signals were detected using chemiluminescence. Membranes were incubated with a sensitive enhanced chemiluminescence detection reagent (Cat No. PK10002, Proteintech, Wuhan, Hubei, China) for 1 minute and then exposed to X-ray film in a chemiluminescence imager.

2.14 Statistical Analysis

Statistical analyses were conducted using GraphPad Prism (version 9.5.0; GraphPad Software, San Diego, CA, USA). Data are expressed as mean ± standard deviation (SD), unless otherwise noted. Two-group comparisons were performed using unpaired two-tailed Student's *t*-tests for normally distributed data and Mann–Whitney *U* tests for non-normally distributed data. For multiple-group comparisons, one-way analysis of variance (ANOVA) with Tukey's post hoc test or the Kruskal–Wallis test was employed. Simple linear regression was applied to evaluate variable correlations, with the coefficient of determination (R^2) and associated *p* value reported. Kaplan–Meier survival curves were compared using the log-rank (Mantel–Cox) test. All *p* values were two-tailed, with statistical significance defined as *p* < 0.05.

3. Results

3.1 Stage-Dependent Remodeling of Macrophage and Epithelial Subtypes Reveals IFIT1$^+$ TAM-CSC Inverse Distribution Pattern

We next analyzed single-cell RNA sequencing (scRNA-seq) data from 10 treatment-naïve patients with epithelial ovarian cancer (EOC). After rigorous quality control and batch effect correction, a total of 36,086 single cells were retained for downstream analysis, including 15,583 cells from early-stage (stage I-II) and 20,503 from advanced-stage (stage III-IV) patients. To assess clinical relevance, we simultaneously analyzed transcriptomic profiles from a cohort of 374 EOC samples in the TCGA database. Dimensionality reduction and clustering revealed 22 distinct cell clusters across all samples (**Supplementary Fig. 1A,B**). Using canonical markers, we annotated seven major cell types: B-plasma cells (*JCHAIN*, *CD79A*), cycling cells (*MKI67*, *TOP2A*), endothelial cells (*CLDN5*, *PLVAP*), epithelial cells (*KRT18*, *EPCAM*, *KRT19*), fibroblasts (*DCN*, *ACTA2*), myeloid cells (*CD14*, *C1QA*), and T cells (*CD3D*, *CD3E*, *CD8A*) (Fig. 1A,C,D). B-plasma cells, endothelial cells, myeloid cells, and T cells were enriched in early-stage tumors, whereas cycling cells, epithelial cells, and fibroblasts were more prevalent in advanced-stage tumors (Fig. 1B). Subclustering was then performed on myeloid and epithelial cells. The myeloid compartment was subdivided into three macrophage subsets (IFIT1$^+$ TAMs, M1, M2), one monocyte subset, and one myeloid dendritic cell subset (Fig. 1E). Notably, the IFIT1$^+$ TAM subpopulation exhibited a resting-like phenotype while concurrently expressing pro-inflammatory cytokines and chemokines (*CCL7*, *IL6*), interferon-stimulated genes

(*IFIT1*, *ISG15*, and *CXCL10*), and M1-associated markers (*CD86*), suggesting a transitional or M1-primed state (Fig. 1F). The M1 subset expressed high levels of *CD86*, *MMP9*, *MARCO*, and *CCL20*. In contrast, M2 macrophages were characterized by expression of the canonical polarization marker musculoaponeurotic fibrosarcoma (*MAF*) [16], but lacked features of IFIT1$^+$ TAMs or M1 phenotypes. Epithelial cells were categorized into one CSC subset and three malignant epithelial subtypes (Fig. 1G), termed Ep-C1, Ep-C2, and Ep-C3. The CSC subset showed strong expression of stemness markers including *CD44*, *THY1*, *ALDH1A1*, and *PROCR* (Fig. 1H). Distinct distribution patterns of macrophage and epithelial subtypes were observed across clinical stages. IFIT1$^+$ TAMs predominated in early-stage patients, whereas M1 and M2 macrophages were enriched in advanced-stage tumors (Fig. 1E). Early-stage tumors were predominantly composed of Ep-C1 and Ep-C2 subtypes, whereas advanced-stage tumors contained higher proportions of CSCs and Ep-C3 cells. These findings highlight stage-dependent remodeling of the tumor microenvironment, characterized by early enrichment of IFIT1$^+$ TAMs and low CSC abundance, contrasting with advanced-stage accumulation of M1/M2 macrophages and CSCs. Given prior studies reporting enhanced invasiveness and stemness in advanced-stage tumors [17], the observed depletion of IFIT1$^+$ TAMs in advanced-stage samples prompted us to further explore a potential inverse relationship between IFIT1$^+$ TAMs infiltration and CSC prevalence. Accordingly, we performed comprehensive analyses to characterize the transcriptional profiles of macrophage and CSC subtypes across tumor stages, validating their clinical relevance using TCGA data and independent patient cohorts.

3.2 Trajectory and Functional Enrichment Analyses Uncover Stage-Dependent Shifts in CSCs and Macrophage Subsets

Pseudotime analysis was carried out using Monocle2 with the DDR-Tree algorithm to reconstruct the epithelial cell lineage trajectory, using Seurat-derived marker genes as input. Branched Expression Analysis Modeling (BEAM) further identified genes linked to fate-determining branch points. As expected, the trajectory positioned CSCs at the origin of the lineage and non-CSC epithelial cells along more differentiated paths, consistent with a stem-to-differentiated transition (Fig. 2A–C). Genes driving trajectory formation are listed in **Supplementary Table 1**. To investigate functional differences across macrophage subpopulations, we conducted pathway enrichment analyses on early- and advanced-stage macrophages. The results revealed distinct transcriptional programs associated with tumor progression and immune modulation (Fig. 2E–G). CSCs were enriched in key oncogenic pathways, including HIF-1 signaling, PI3K-Akt signaling, ECM–receptor interaction, and platinum drug resistance—well-established regulators of stemness maintenance, proliferation, and chemoresistance [18,19,20,21,22], underscoring their pivotal role in EOC progression (Fig. 2D). Early-stage IFIT1$^+$ TAMs were enriched for immune activation pathways such as antigen processing and presentation, lysosome, and phagosome, indicative of intact tumor recognition and clearance functions. These findings are consistent with an effective immune surveillance state characteristic of early-stage tumors. Strikingly, instead of adopting classical pro-tumoral programs, advanced-stage IFIT1$^+$ TAMs showed strong enrichment in pathways with potential anti-tumor activities, including nuclear factor kappaB (NF-κB) signaling, Toll-like receptor (TLR) signaling, leukocyte transendothelial migration, and complement activation. Likewise, advanced-stage M1 and M2 macrophages also upregulated these complex inflammatory pathways without exhibiting canonical pro-tumoral signatures. This indicates that macrophages in late-stage EOC mount a highly intricate and sustained inflammatory response, rather than undergoing simple pro-tumoral polarization. Taken together, these findings suggest that macrophage activation states evolve with tumor progression, exhibiting stage-dependent rewiring of immune and inflammatory programs. In particular, IFIT1$^+$ TAMs appear as a functionally distinct subset characterized by immune vigilance in early-stage disease and by a complex, chronic inflammatory signature in advanced-stage tumors. These results reinforce the notion that the functional polarization of macrophage subsets, especially IFIT1$^+$ TAMs, is tightly linked to the dynamic tumor microenvironment during EOC progression.

3.3 IFIT1$^+$ TAMs Depletion and Signature-Based Survival Analysis Associate With Advanced EOC and Poor Prognosis

Using the CIBERSORT algorithm, we examined immune cell composition across ovarian cancer stages I–IV and detected marked stage-dependent shifts in macrophage subsets (Fig. 3A). Specifically, IFIT1$^+$ TAMs infiltration progressively decreased from stage I to IV, whereas M2 macrophages significantly increased, particularly in stages III and IV ($p < 0.05$). In contrast, M1 macrophages showed no notable change across stages, suggesting distinct roles of IFIT1$^+$ TAMs and M2 subsets in disease progression.

To robustly assess the prognostic value of macrophage subsets and mitigate the unreliability of single-gene evaluations, we performed Kaplan–Meier survival analysis utilizing multi-gene signature scoring. The analysis revealed that high expression of *IFIT1*, a marker of IFIT1$^+$ TAMs, was significantly associated with prolonged overall survival (log-rank $p = 0.0152$, HR = 0.689, 95% CI: 0.51–0.931), indicating a protective role of IFIT1$^+$ TAMs in EOC (Fig. 3B). Conversely, elevated expression of *CD86* (M1 marker) and *MAF* (M2 marker) correlated with poorer prognosis (*CD86*: $p = 0.00525$, HR = 1.646; *MAF*: $p = 0.00656$, HR

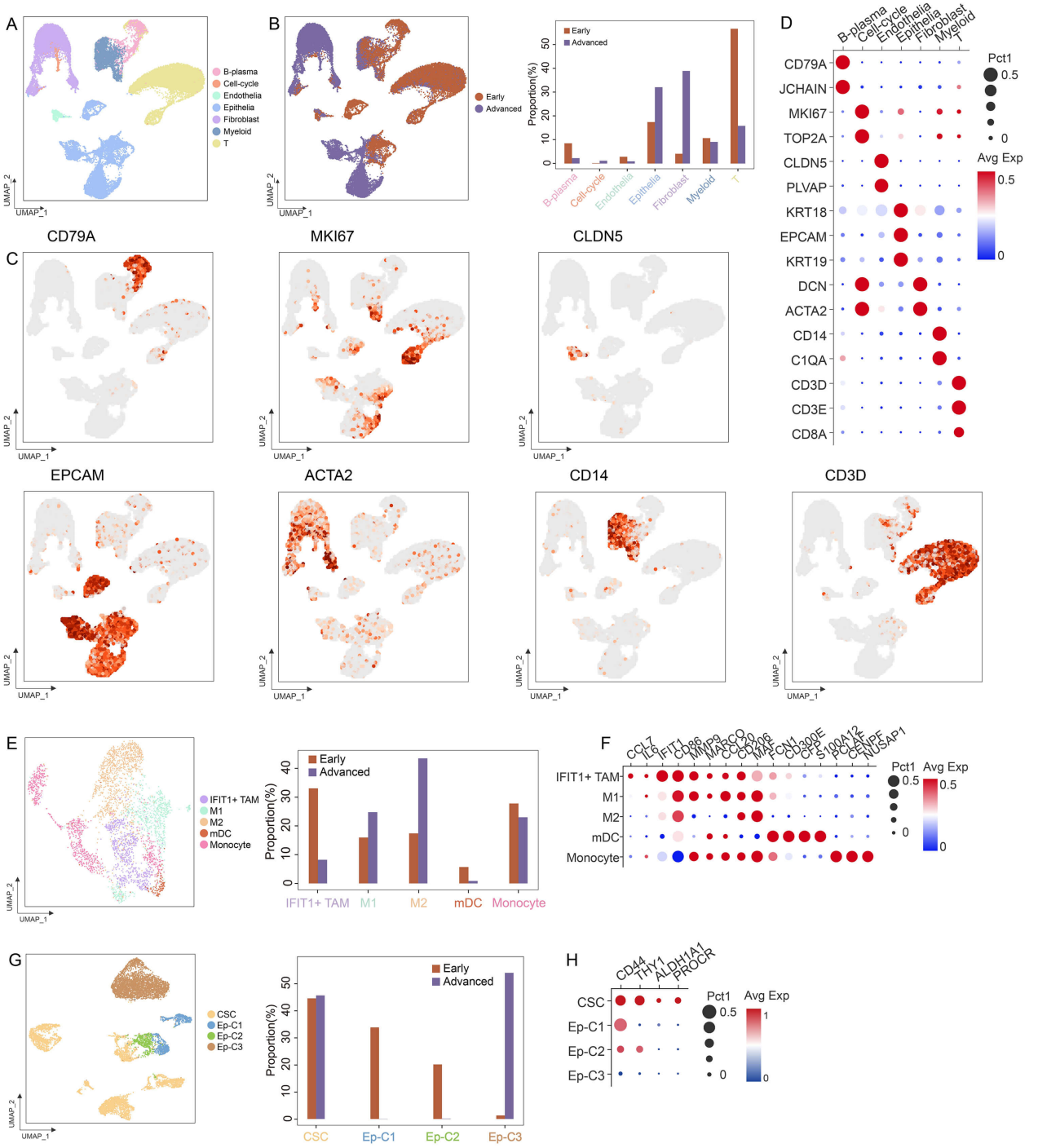


Fig. 1. Single-cell analysis reveals a significant association between IFIT1$^+$ tumor-associated macrophages (TAMs) and the staging of epithelial ovarian cancer (EOC). (A) Uniform Manifold Approximation and Projection (UMAP) visualization of 7 cell types. Colors represent different cell types. (B) UMAP plot showing the distribution of cells from early- and advanced-stage EOC samples (left), and a bar graph illustrating cell type proportions across stages (right). (C) Cell type-specific gene marker expression visualized using UMAP. Higher levels of expression are indicated by redder colors. (D) Dot plot showing marker gene expression across different cell types. The size of the dots is proportional to abundance, and the color represents expression level. (E) UMAP showing subclusters of myeloid cells (left), and bar plot showing stage-specific proportions of each myeloid subset (right). (F) Dot plot depicting marker gene expression in myeloid cells. The size of the dots is related to their abundance, and the color denotes the expression level. (G) UMAP showing epithelial subclusters (left), and bar plot displaying the proportions of each epithelial subtype by tumor stage (right). (H) Dot plot depicting marker gene expression in epithelial cells. The size of the dots is related to their abundance, and the color denotes the expression level. IFIT1$^+$, interferon-induced protein with tetratricopeptide repeats 1$^+$.

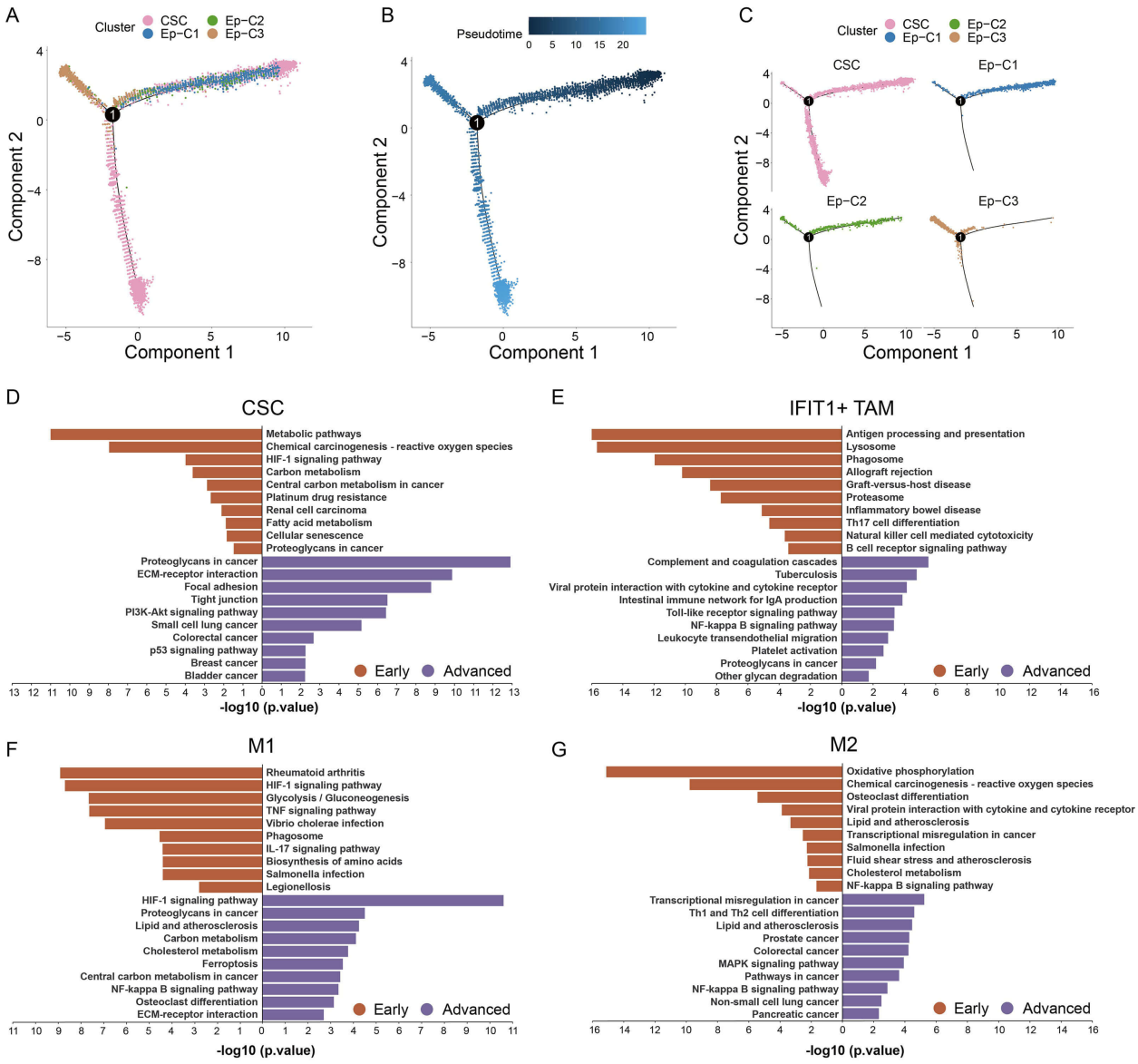


Fig. 2. Trajectory and functional enrichment analyses reveal distinct biological programs in cancer stem cells (CSCs) and macrophage subsets, highlighting IFIT1$^+$ TAM as a functionally unique population. (A) Pseudo-time trajectory analysis of the four sub-clusters of epithelial cells. (B) The progression of cells along a developmental path, with colors representing pseudotime states. (C) Pseudo-time trajectory of cells in each epithelial cell cluster. (D–G) Pathway enrichment analysis for CSCs (D), IFIT1$^+$ TAM (E), M1 macrophages (F), and M2 macrophages (G), showing significantly enriched pathways ranked by -log10 (adjusted *p*-value).

= 1.612), implying that M1 and M2 macrophages may contribute to tumor aggressiveness.

We next analyzed the expression of four CSC markers—*ALDH1A1*, *CD44*, *PROCR*, and *THY1*—across different tumor stages (Fig. 3C). *THY1* expression was significantly elevated in stages III and IV compared to stage II ($p < 0.05$), while the others showed no significant variation. Kaplan–Meier survival analysis further revealed that high expression of *PROCR* ($p = 0.0179$, HR = 1.54) and *THY1* ($p = 0.00104$, HR = 1.585) was associated with worse overall survival, whereas *ALDH1A1* and *CD44* were not prognostic (Fig. 3D).

Correlation analysis revealed no statistically significant associations between the IFIT1$^+$ TAMs signature and the four CSC markers (*ALDH1A1*, *CD44*, *PROCR*, *THY1*; all $p > 0.05$) (Fig. 3E). In contrast, the M1 signature expression was positively correlated with *ALDH1A1*, *CD44*, and *PROCR* (Fig. 3F), while the M2 signature was significantly correlated with all four CSC markers (Fig. 3G). These results suggest that M1 and M2 macrophages may support CSC maintenance, whereas IFIT1$^+$ TAMs do not.

To further validate these findings, immunohistochemical staining was performed on tumor samples from 20 EOC patients (**Supplementary Table 2**). IFIT1 and CD44 served as markers for IFIT1$^+$ TAMs and CSCs, respectively

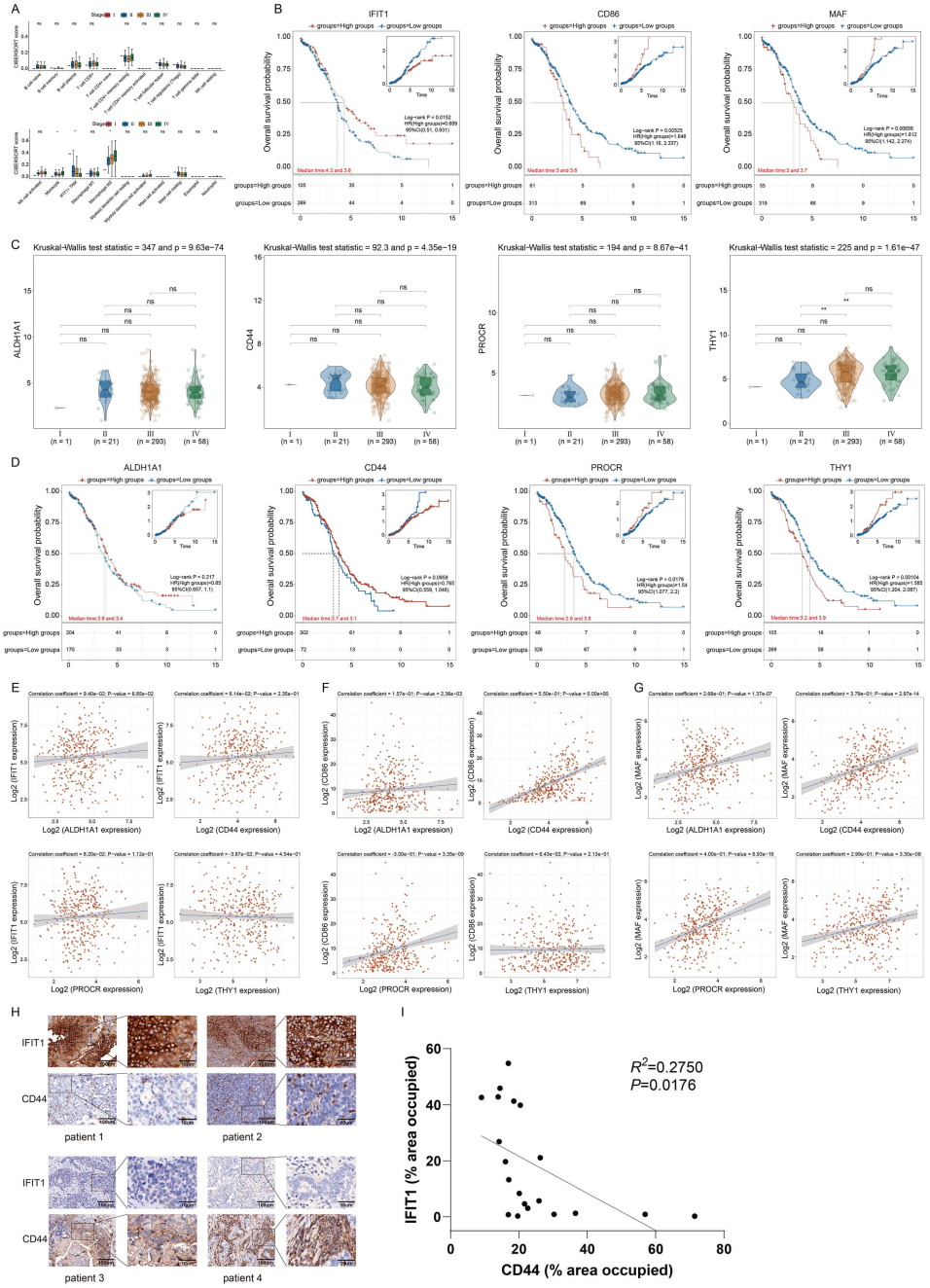


Fig. 3. Reduced IFIT1$^+$ TAMs infiltration and IFIT1 expression are associated with advanced EOC stage, unfavorable prognosis, and elevated CSC marker expression. (A) Distribution of immune cell proportions across ovarian cancer stages (I–IV) based on Cell-type Identification by Estimating Relative Subsets of RNA Transcripts (CIBERSORT) analysis. (B) Kaplan-Meier survival analysis of IFIT1, CD86 and MAF in ovarian cancer. (C) Expression levels of cancer stem cell markers across different stages of ovarian cancer. (D) Kaplan-Meier survival analysis of cancer stem cell markers in ovarian cancer. (E) Correlation analysis between IFIT1 (IFIT1$^+$ TAMs marker) and cancer stem cell markers in ovarian cancer. (F) Correlation analysis between CD86 (M1 macrophage marker) and cancer stem cell markers in ovarian cancer. (G) Correlation analysis between MAF (M2 macrophage marker) and cancer stem cell markers in ovarian cancer. Statistical significance is denoted as *$p < 0.05$, **$p < 0.01$, ns, not significant. Scale bars: 100 μm (main images), 10 μm (insets). (H) Representative immunohistochemical staining of IFIT1 and CD44 in ovarian cancer tissue from four patients. (I) Negative correlation between IFIT1 and CD44 expression in ovarian cancer tissues ($R^2 = 0.2750$, $p = 0.0176$). MAF, musculoaponeurotic fibrosarcoma.

(Fig. 3H). Quantitative ROI analysis showed a significant negative correlation between IFIT1 and CD44 expression ($R^2 = 0.2750$, $p = 0.0176$; Fig. 3I), indicating that increased IFIT1$^+$ TAMs infiltration is associated with reduced CSC presence, and suggesting a potential tumor-suppressive role of this specific TAM subpopulation in the EOC microenvironment.

3.4 Stage-Dependent Shifts in Macrophage-CSC Signaling Dynamics Reveal Early-IFIT1$^+$ TAM-Mediated Tumor Suppression

The roles of M1 and M2 macrophages in promoting cancer stemness have been relatively well established, with both shown to enhance tumor cell stemness [23,24]. However, the impact of IFIT1$^+$ TAMs on cancer stemness remains insufficiently studied. Therefore, our focus is on investigating the effects of IFIT1$^+$ TAMs on the stemness of tumor cells.

EOC progression involves complex interactions between macrophage subsets and other cell types. To clarify the coordinated cellular responses during tumor progression or macrophage polarization, we performed a quantitative analysis of potential cell–cell communications across all cell types in early versus advanced EOC niches using a published ligand–receptor database (Fig. 4A,B). While early-stage samples exhibited globally elevated intercellular signaling activity, late-stage CSCs demonstrated significantly strengthened interactions with multiple immune cell subsets, suggesting a potential role in actively orchestrating immune modulation to promote immune evasion. Although total interaction strength between CSCs and macrophage subsets (IFIT1$^+$ TAM, M1, M2) was not the most prominent, IFIT1$^+$ TAMs–CSC interactions were significantly more frequent in early samples (Fig. 4C).

To further characterize the ligand–receptor interaction features and potential regulatory mechanisms between macrophage subtypes at different developmental stages and CSCs, we performed a systematic CellPhoneDB analysis [25] of intercellular signaling between six macrophage subsets (early-stage IFIT1$^+$ TAMs, early-M1, early-M2, advanced-stage IFIT1$^+$ TAMs, advanced-M1, advanced-M2) and CSCs (Fig. 4D).

The results revealed several specific interaction axes between early-stage IFIT1$^+$ TAMs and early-CSCs, including TNFSF10–TNFRSF10A/B, Cholesterol_byLIPA–RORA, and FPR3–HEBP1. Among these, the TNFSF10–TNFRSF10A/B axis represents a classical apoptosis-inducing pathway, suggesting that early-stage IFIT1$^+$ TAMs may trigger CSC apoptosis through activation of the DR4/5 signaling cascade. Additionally, RORA and HEBP1—both known CSC suppressors—were paired with ligands Cholesterol_byLIPA and FPR3, which were highly expressed in early-stage IFIT1$^+$ TAMs. This implies that early-stage IFIT1$^+$ TAMs may secrete specific metabolic and chemotactic factors to drive CSCs toward a non-stem-like state, thereby exerting tumor-suppressive effects within the early tumor niche.

Distinct interaction patterns were likewise evident across other macrophage subtypes. Early-M1 macrophages displayed robust signaling crosstalk with early-CSCs via pro-inflammatory axes including IL1B–IL1R and growth factor pathways such as VEGFA–NRP1/2, with ligands and receptors abundantly expressed. These findings suggest that early-M1 macrophages may modulate CSC biology through diverse molecular mechanisms. Notably, the IL1B–IL1R axis, in addition to mediating inflammatory responses, has been implicated in enhancing CSC stemness, inducing epithelial-mesenchymal transition (EMT), promoting invasion and metastasis, and facilitating immune evasion [26,27]. Meanwhile, VEGFA–NRP1/2 signaling may contribute to tumor progression by promoting angiogenesis, sustaining CSC properties, and shaping an immunosuppressive microenvironment [28,29,30].

Early-M2 macrophages showed strong activation of canonical signaling axes with early-CSCs, notably TGFB2–TGFBR3 and CX3CR1–CX3CL1, encompassing pivotal transforming growth factors and chemokines. The TGF-β family is known to promote EMT, metastasis, and immunosuppression, thereby supporting CSC maintenance [31,32]. CX3CL1 not only enhances cancer cell invasiveness [33] but also facilitates Treg infiltration and activation, contributing to the formation of an immunosuppressive microenvironment [34].

In advanced-stage tumors, macrophage–CSC interactions shift significantly. Critically, interactions between advanced-stage IFIT1$^+$ TAMs and CSCs transition from the pro-apoptotic TNFSF10–TNFRSF10B axis to dominance of the TNFSF12/15–TNFRSF25 pathway. This shift fundamentally alters the functional dynamics, as TNFRSF25 signaling primarily regulates cell survival, proliferation, and inflammatory adaptability instead of triggering apoptosis. This pivotal switch likely underlies the diminished tumor-suppressive capacity of advanced-stage IFIT1$^+$ TAMs. Furthermore, advanced-M1–CSC interactions are dominated by proliferative (VEGFA–NRP1/2, WNT5A–FRZB, JAG1–NOTCH3) and inflammatory (IL1A–IL1R) signals. Advanced-M2 engages CSCs through growth factor (HBEGF–EGFR, TGFB2–TGFBR3) and chemokine (CX3CR1–CX3CL1, CCL3–ACKR2) pathways, supporting CSC maintenance and tumor progression. Overall, early-stage IFIT1$^+$ TAMs communicates with CSCs via pro-apoptotic, inhibitory signals, while this function is lost in advanced-stage IFIT1$^+$ TAMs and replaced by survival-promoting signals and M2-driven pro-CSC signaling. This shift suggests IFIT1$^+$ TAM-CSC interactions may regulate CSC plasticity during tumor evolution.

To validate the stage-specific expression patterns of IFIT1$^+$ TAM–CSC interaction-related genes, we analyzed the expression levels of *HEBP1*, *RORA*, and *TNFRSF10B* across different pathological grades of ovarian cancer (G1–

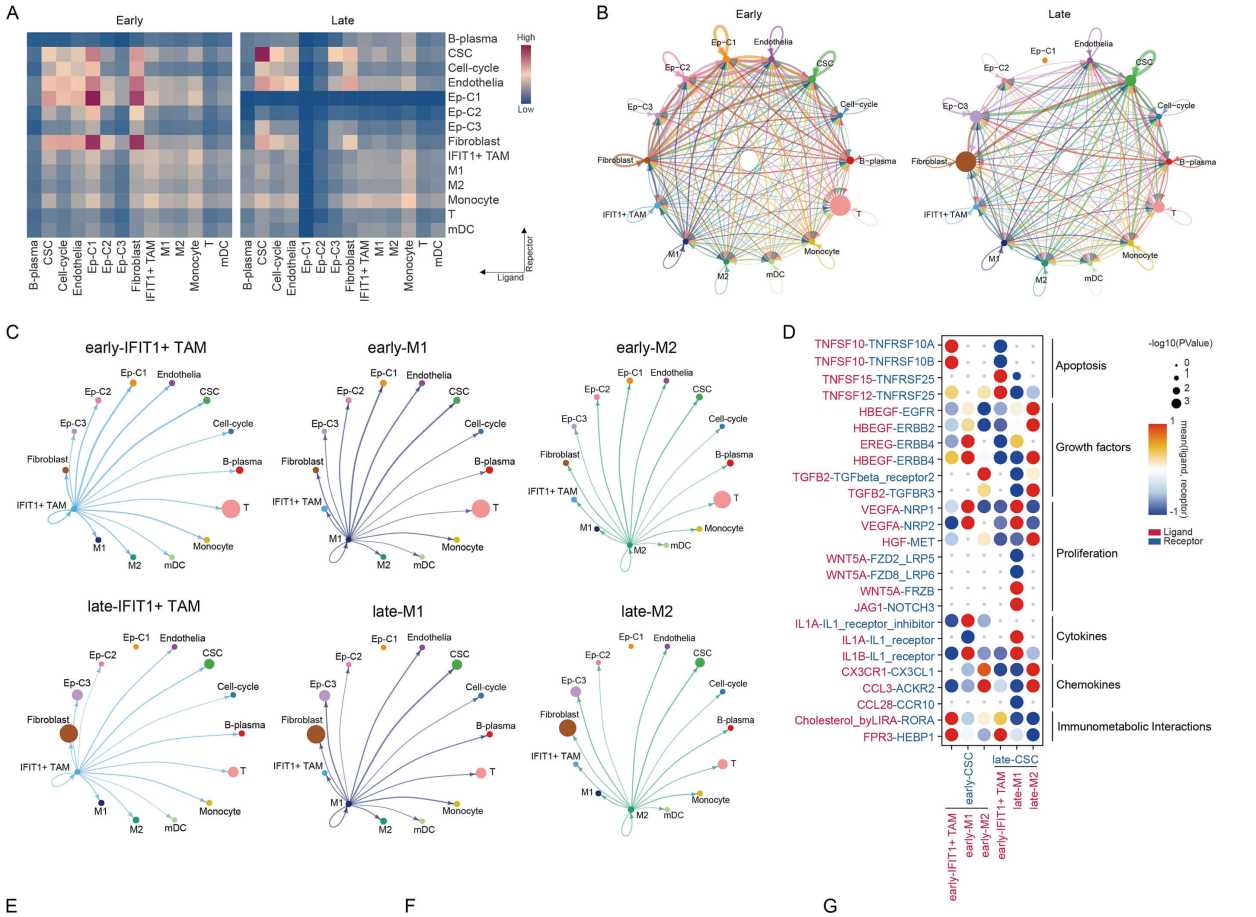


Fig. 4. Loss of IFIT1$^+$ TAM-associated inhibitory signaling promotes CSC maintenance and immune evasion in advanced EOC. (A) Heatmaps showing ligand-receptor interaction strength among all cell types in early and advanced EOC. (B) Circle plots illustrating global intercellular communication networks; edge width reflects the number of ligand-receptor pairs. (C) Outgoing interaction patterns from each macrophage subset to other cell types; arrow width indicates interaction strength. (D) Dot plot of significant macrophage-CSC ligand-receptor pairs. Dot size indicates -log10(p), and color denotes expression level. (E–G) Violin plots showing expression levels of *HEBP1*, *RORA*, and tumor necrosis factor receptor superfamily member 10B (*TNFRSF10B)* across tumor grades and normal ovary. Statistical significance is denoted as *$p < 0.05$ and ****$p < 0.0001$, ns, not significant.

G4) and normal ovarian tissues (Fig. 4E–G). Violin plot analysis revealed that all three genes exhibited significantly higher expression levels in normal tissues than in tumor samples. Notably, *RORA* and *TNFRSF10B* expression was markedly reduced in high-grade tumors (G3–G4) relative to normal controls. These findings support the notion that the loss of IFIT1$^+$ TAM-associated inhibitory signaling—particularly the TNFSF10–TNFRSF10B apoptotic axis and the nuclear receptor RORA—may contribute to the maintenance of cancer stem cells and enhanced immune evasion in advanced epithelial ovarian cancer.

3.5 M0 Macrophages Attenuate Multidrug Resistance and Stemness in EOC Cells and Upregulate TNFRSF10B *Expression*

Trajectory analyses indicate that interferon-responsive TAMs (e.g., IFIT1$^+$) represent an early transitional state closely linked to monocytic origins [35]. Since both M0 macrophages and these early-stage TAMs share a similar uncommitted status prior to terminal polarization, unpolarized M0 cells serve as a surrogate to model their baseline properties in vitro. To establish the baseline functional impact of M0 macrophages on cancer stemness, we utilized a THP-1-derived co-culture model. THP-1 monocytes were induced to differentiate into M0 macrophages through PMA stimulation (Fig. 5A), and their polarization status, alongside subsequent M1 and M2 induction, was rigorously validated using CD86 and CD206 surface markers via flow cytometry, confirming well-defined macrophage phenotypic identities (Fig. 5B).

Conditioned media (CM) derived from these macrophage subsets were applied to EOC cell lines (SKOV3, HEY, and A2780) to observe their modulation of the tumor microenvironment. CCK-8 assays demonstrated that M0-CM significantly improved EOC chemosensitivity to doxorubicin, docetaxel, and carboplatin across multiple concentration gradients, substantially surpassing the control, M1-CM, and M2-CM groups (Fig. 5C–E). This suggests that M0 macrophages possess a unique regulatory capability to modulate chemo-responsiveness, independent of canonical M1- or M2-associated inflammatory profiles. Flow cytometry further confirmed a pronounced reduction in the CD44$^+$ stem-like subpopulation among M0-CM-treated EOC cells (Fig. 5F,G), aligning with our phenotypic observations. Correspondingly, spheroid formation assays in serum-free suspension revealed a significant decrease in spheroid-forming potential after M0-CM exposure, suggesting suppression of stemness-associated self-renewal (Fig. 5H).

To elucidate the underlying mechanisms of this suppressive phenotype, we conducted qRT-PCR and Western blot analyses targeting candidate receptors identified through prior ligand–receptor screening. These results established that M0-CM treatment specifically upregulated the expression of DR5 at both the mRNA and protein levels across all three EOC cell lines (Fig. 5I,J). Notably, *HEBP1* and *RORA* were two other candidate receptors identified from the scRNA-seq screening. However, their expression levels remained unchanged with no significant variation across treatment groups. Collectively, these results highlight the intrinsic ability of M0 to suppress CSC properties and induce DR5 expression, establishing a strong foundation for investigating the TNF-related apoptosis-inducing ligand (TRAIL)-DR5 axis as the key molecular mediator of this tumor-suppressive effect *in vivo*.

3.6 TRAIL Restricts EOC Stemness and Reverses Chemoresistance Specifically Through the DR5 Receptor

Guided by the scRNA-seq finding that the TRAIL ligand is highly enriched in IFIT1$^+$ TAMs, along with our *in vitro* observation of DR5 induction in EOC cells following M0-CM exposure, we proposed that the TRAIL-DR5 axis acts as the central regulatory pathway governing cancer stemness. To validate this hypothesis, we generated targeted si-DR5 knockdown models in SKOV3, HEY, and A2780 cell lines. Western blotting combined with densitometric analysis confirmed effective suppression of DR5 protein levels (Fig. 6A,B).

To assess the specific role of the TRAIL-DR5 axis in modulating the CSC population, flow cytometry was carried out with or without exogenous TNFSF10. Flow cytometry revealed that exogenous TNFSF10 treatment significantly depleted the CD44$^+$ population in NC (negative control) cells. Critically, this depleting effect was abolished in si-DR5 cells, which retained a significantly greater proportion of CD44$^+$ stem-like cells under the same conditions (Fig. 6C). Parallel evaluation of a secondary CSC marker, CD90, demonstrated a consistent trend. Specifically, DR5 silencing effectively reversed the TNFSF10-induced reduction of the CD90$^+$ population, thereby maintaining a significantly higher proportion of CD90$^+$ cells in the si-DR5 cohort (**Supplementary Fig. 2**).

To further assess the clinical implications of multidrug resistance, EOC cells (NC and si-DR5) were exposed to TNFSF10 in combination with increasing concentrations of carboplatin, docetaxel, or doxorubicin. CCK-8 assays demonstrated that TNFSF10 markedly enhanced the sensitivity of NC EOC cells to all examined chemotherapeutic agents. In contrast, DR5 knockdown substantially diminished this sensitizing effect, leading to restored cell viability and multidrug resistance. A specific deviation was observed in A2780 cells treated with 2 μM and 4 μM doxorubicin, where the si-DR5 group exhibited lower viability compared to the NC group. Despite this localized variance, the overall statistical trend across the broader concentration gradients and all three cell lines consistently demonstrated that DR5 knockdown preserved cell viability and multidrug resistance (Fig. 6D–F). These findings confirm that exogenous TNFSF10 suppresses EOC stem-like properties and boosts chemosensitivity, with this inhibitory effect strictly reliant on the downstream DR5 receptor. Our findings identify the TRAIL-DR5 signaling axis as a pivotal regulatory mechanism through which IFIT1$^+$ TAMs exert their tumor-suppressive functions, highlighting its potential as a therapeutic target to overcome CSC-mediated chemoresistance in advanced EOC.

4. Discussion

EOC presents a profound clinical challenge driven by pronounced intra-tumoral heterogeneity and a highly immunosuppressive TME [36,37]. Within this niche, CSCs

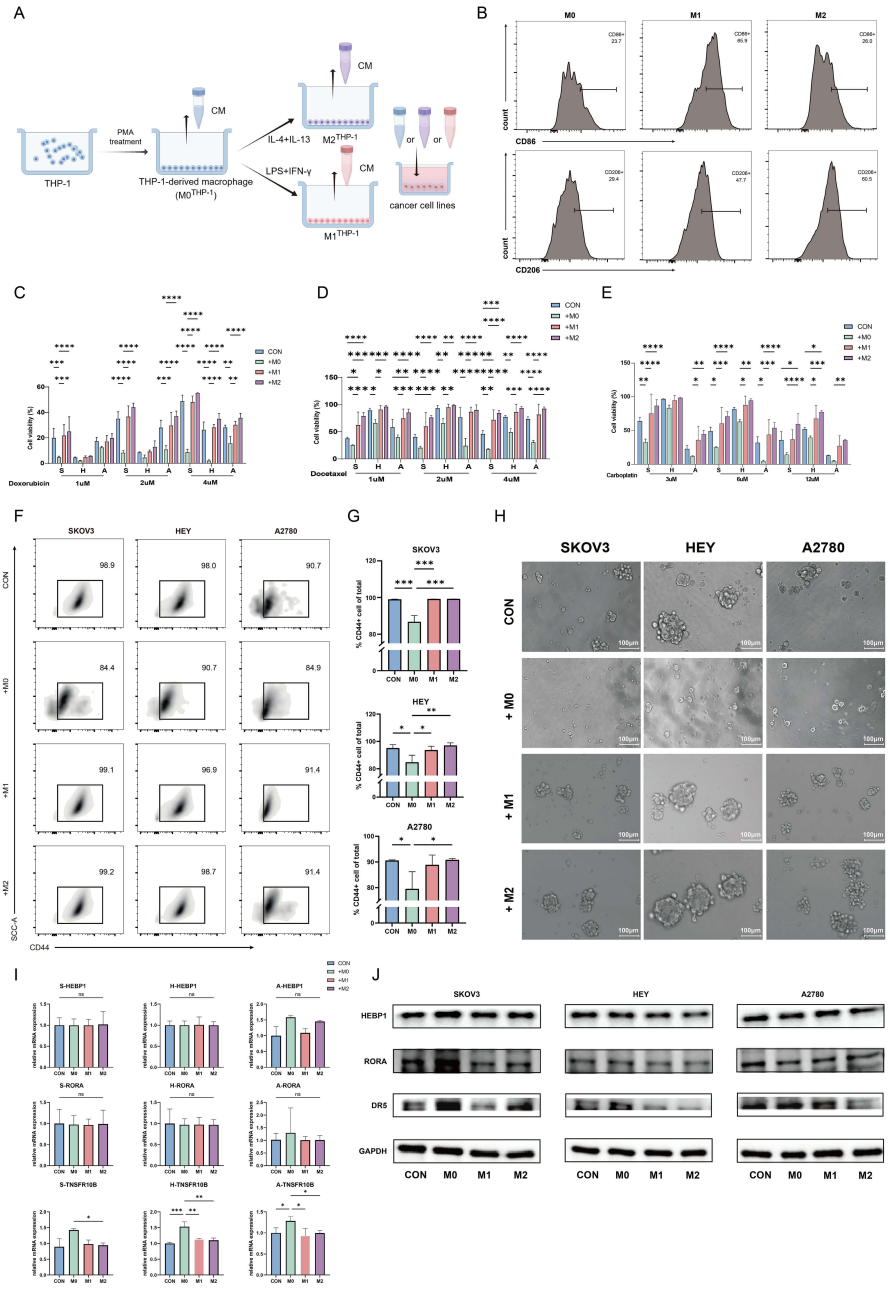


Fig. 5. M0 macrophages attenuate multidrug resistance and stemness in EOC cells by upregulating TNFRSF10B. (A) Schematic of THP-1 macrophage polarization and the conditioned media (CM) co-culture model. (B) Flow cytometry analysis validating the polarization status of THP-1-derived M0, M1, and M2 macrophages using CD86 and CD206 markers. (C–E) Cell Counting Kit-8 (CCK-8) assay assessing the cell viability of EOC cell lines (SKOV3, HEY, and A2780) treated with doxorubicin (C), docetaxel (D), or carboplatin (E) across various concentrations in the presence of macrophage CM. Data are presented as mean ± standard deviation (SD) (n = 3). (F,G) Flow cytometry analysis (F) and corresponding quantification (G) of $CD44^{+}$ cancer stem-like populations in EOC cells following treatment with CM from distinct macrophage subsets (n = 3). (H) Spheroid formation assays evaluating the enrichment of CSCs in serum-free suspension cultures across different CM conditions. Images were captured at 20× magnification. Scale bars: 100 µm. (I,J) Quantitative real-time polymerase chain reaction (qRT-PCR) (I) and Western blot (J) analyses of tumor necrosis factor receptor superfamily member 10B (Death receptor 5) (TNFRSF10B/DR5), HEBP1, and RORA expression at the mRNA and protein levels in SKOV3, HEY, and A2780 cell lines following M0-CM treatment, compared to control, M1-CM, and M2-CM groups. Statistical significance: *$p < 0.05$, **$p < 0.01$, ***$p < 0.001$, ****$p < 0.0001$, ns, not significant.

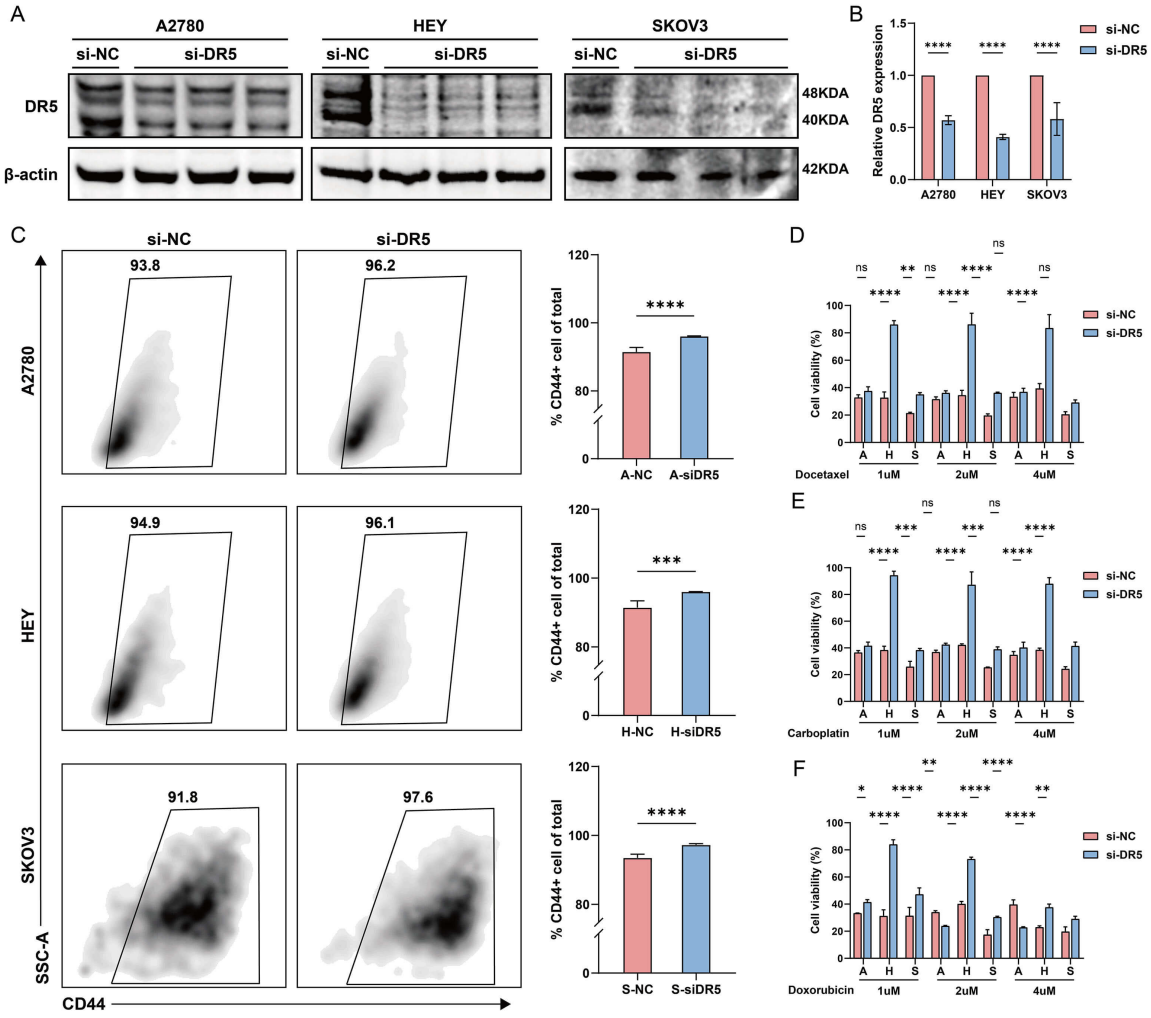


Fig. 6. Exogenous tumor necrosis factor ligand superfamily member 10 (TNFSF10) suppresses cancer stemness and enhances chemosensitivity via the TNFRSF10B receptor. (A) Western blot analysis confirming the knockdown efficiency of DR5 in SKOV3, HEY, and A2780 cell lines using specific siRNA. (B) Quantitative grayscale analysis of DR5 protein expression normalized to β-actin. (C) Flow cytometry analysis and quantification of CD44+ cells in si-NC and si-DR5 EOC cells following TNFSF10 treatment. (n = 5). (D–F) CCK-8 cell viability assays of si-NC and si-DR5 EOC cells exposed to TNFSF10 combined with gradient concentrations of docetaxel (D), carboplatin (E), and doxorubicin (F). (n = 3). Statistical significance is denoted as $*p < 0.05$, $**p < 0.01$, $***p < 0.001$, and $****p < 0.0001$, ns, not significant. Si-NC, small interfering RNA negative control.

act as the primary engines of tumor recurrence and multidrug resistance [38]. While TAMs are known to critically orchestrate EOC progression, their precise regulatory impact on the CSC compartment remains incompletely understood [39,40]. In this study, integrated single-cell transcriptomic and *in vitro* functional analyses uncover a stage-specific decline in IFIT1$^+$ TAMs during EOC progression. We demonstrate that these specific interferon-responsive macrophages maintain an inverse spatial and functional relationship with CSCs, fundamentally restricting cancer stemness and enhancing chemosensitivity through the TRAIL–DR5 signaling axis in early-stage disease.

Our findings contribute to a necessary paradigm shift in understanding macrophage plasticity, moving beyond the traditional, rigid binary division of M1 (antitumor) and M2 (protumor) activation states [41,42]. Historically, functional investigations have frequently relied on traditional *in vitro* systems where unpolarized cells (M0) were conceptualized merely as biologically inert precursors [43]. Interestingly, our preliminary *in vitro* co-culture screening indicated a baseline capacity of these M0 to restrict EOC stem-like traits. High-resolution *in vivo* single-cell RNA sequencing further elucidated this observation, showing that the tumor-suppressive function is naturally carried out by IFIT1$^+$ TAMs. Consistent with recent pan-cancer single-cell landscapes [35,44,45], these IFIT1$^+$ TAMs represent a specialized, interferon-primed intermediate state nestled within the M1-activation spectrum, characterized by a ro-

bust ISG signature (including IFIT1, ISG15, and CXCL10) [46,47]. This highlights that the anti-CSC vigilance in early EOC is driven by a highly specialized, immune-active subpopulation rather than generic quiescent macrophages, which aligns with our *in vitro* observation that baseline M0 suppress CSC traits prior to alternative polarization.

To comprehensively capture the dynamic remodeling of the tumor microenvironment (TME), it is essential to decipher the transcriptomic evolution of these macrophages during tumor progression. In late-stage EOC, IFIT1$^+$ TAMs—alongside classical M1 and M2 subsets—exhibited profound enrichment in pathways conventionally linked to active inflammation, including NF-κB signaling, TLR signaling, and complement cascades. While these pathways are canonically associated with acute pathogen clearance [48], their chronic upregulation in advanced TMEs must not be simplistically interpreted as a pro-tumoral polarization. Instead, recent spatially resolved and single-cell studies demonstrate that persistent and unresolved activation of inflammatory networks drives a state of chronic, dysregulated low-grade inflammation [49,50]. Such maladaptive inflammatory signaling disrupts vascular integrity, depletes local immune effectors, and establishes an increasingly immunosuppressive milieu, thereby undermining the ability of mature macrophages to constrain the neighboring cancer stem cell (CSC) niche.

This functional decline is further underscored by a pronounced shift in intercellular communication patterns. CellPhoneDB analysis revealed that early-stage IFIT1$^+$ TAMs specifically engage CSCs through the pro-apoptotic TNFSF10–TNFRSF10B (TRAIL–DR5) axis. However, advanced-stage macrophages abandon this axis, pivoting exclusively toward the TNFSF15–TNFRSF25 axis. This ligand-receptor switch profoundly reshapes the selective pressures within the TME. Unlike TRAIL, which effectively forces apoptotic execution [51], signaling through TNFRSF25 mediated by ligands such as TNFSF15 predominantly drives downstream inflammatory responses, cellular survival, and adaptive microenvironmental remodeling. Basic experimental models have demonstrated that TNFSF15–TNFRSF25 interaction activates NF-κB signaling and upregulates angiogenic factors like VEGF-C, thereby facilitating tumor metastasis rather than apoptosis [52]. As a result, this pivotal receptor transition may abolish the intrinsic tumor-suppressive function of macrophages, enabling uncontrolled expansion of CSCs in advanced disease.

The therapeutic potential of targeting the TNFSF10–TNFRSF10B axis is heavily supported by our targeted *in vitro* validations and extensive prior research across diverse solid malignancies. By utilizing rhTRAIL and targeted siRNA silencing, we confirmed that DR5 is a critical mechanistic mediator for suppressing EOC stem-like properties and reversing multidrug resistance. Given that CD44 represents a key therapeutic target and stemness marker driving solid tumor progression [53], the observed reduction in the CD44$^+$ subpopulation observed in our study highlights the clinical relevance of this axis. Selective eradication of the CSC population via the DR5 pathway has likewise been achieved through diverse exogenous delivery platforms. These approaches include mesenchymal stem cell-delivered TRAIL [54], engineered chimeric antigen receptor macrophages (CAR-Ms) [55], and small-molecule inducers like ONC201/TIC10 [56,57]. Whereas our *in vitro* experiments relied on exogenous recombinant proteins to confirm receptor dependence, our single-cell profiling uniquely indicates that IFIT1$^+$ TAMs naturally function as endogenous cellular vehicles, intrinsically equipped to deliver these suppressive signals directly and locally to the CSC niche *in vivo*.

From a translational perspective, the IFIT1$^+$ TAM signature and its associated secretory profile may serve as a reliable prognostic biomarker for EOC [58], guiding stratified interventions. As the protective TNFSF10–TNFRSF10B apoptotic pathway is disrupted in late-stage disease, therapeutic strategies aimed at locally reprogramming the myeloid compartment toward a persistent, interferon-primed IFIT1$^+$ state—potentially in combination with standard chemotherapeutics like carboplatin or paclitaxel—could effectively eliminate the chemoresistant CSC pool and prevent recurrence [59]. Future mechanistic studies must prioritize identifying the exact upstream molecular cues that govern the pathological switch from the TRAIL to the Tumor necrosis factor-like weak inducer of apoptosis (TWEAK) signaling axis during microenvironmental remodeling.

5. Limitations

Several limitations warrant explicit acknowledgment. First, our *in vitro* validations were based on targeted siRNA knockdown and recombinant protein application, without *in vivo* confirmation or direct measurement of endogenous TNFSF10 secretion from primary IFIT1$^+$ TAMs. Since recombinant proteins cannot fully recapitulate physiological concentration gradients and release kinetics within the tumor microenvironment, future investigations employing conditional knockout models are essential. Second, transcriptomic analyses relied on retrospective cohorts with small sample sizes; thus, prospective validation in larger, well-powered clinical cohorts is needed to establish the prognostic significance of the IFIT1$^+$ TAM signature. Third, this study was restricted to HGSOC, making it uncertain whether these TAM–CSC interactions extend to other EOC histotypes. Finally, the possible synergistic or inhibitory roles of neighboring immune cells—including dendritic cells or defined regulatory T cell subsets—in modulating the TNFSF10–TNFRSF10B pathway remain unexplored and merit systematic examination.

6. Conclusions

In summary, this study outlines a stage-dependent depletion of IFIT1$^+$ TAMs during EOC progression and establishes their tumor-suppressive role in the early malignant niche. By integrating single-cell transcriptomics with targeted *in vitro* functional analyses, we reveal that these specific interferon-responsive macrophages are intrinsically programmed to restrict cancer stemness. Crucially, our molecular validations using recombinant TNFSF10 and receptor silencing demonstrate that the attenuation of EOC stem-like properties and multidrug resistance is dependent on the downstream TNFRSF10B/DR5. These insights clarify macrophage functional heterogeneity, suggesting that polarizing TAMs toward a persistent, interferon-primed IFIT1$^+$ state offers a viable therapeutic strategy to eliminate the resilient CSC pool in EOC.

Abbreviations

EOC, Epithelial ovarian cancer; CSC(s), Cancer stem cell(s); TME, Tumor microenvironment; TAMs, Tumor-associated macrophages; TNFSF10 (TRAIL), Tumor necrosis factor ligand superfamily member 10 (TNF-related apoptosis-inducing ligand); TNFRSF10B (DR5), Tumor necrosis factor receptor superfamily member 10B (Death receptor 5); TCGA, The Cancer Genome Atlas; GEO, Gene Expression Omnibus; scRNA-seq, Single-cell RNA sequencing; ISGs, Interferon-stimulated genes; UMAP, Uniform Manifold Approximation and Projection; PCA, Principal component analysis; BEAM, Branched expression analysis modeling; FDR, False discovery rate; DEG(s), Differentially expressed gene(s); GO, Gene Ontology; KEGG, Kyoto Encyclopedia of Genes and Genomes; CIBERSORT, Cell-type Identification by Estimating Relative Subsets of RNA Transcripts; DMEM, Dulbecco's Modified Eagle Medium; FBS, Fetal bovine serum; PMA, Phorbol 12-myristate 13-acetate; LPS, Lipopolysaccharide; IFN-γ, Interferon-gamma; CM, Conditioned medium; CCK-8, Cell Counting Kit-8; PBS, Phosphate-buffered saline; qRT-PCR, Quantitative real-time polymerase chain reaction; RIPA, Radioimmunoprecipitation assay; BCA, Bicinchoninic acid; SDS-PAGE, Sodium dodecyl sulfate–polyacrylamide gel electrophoresis; TBST, Tris-buffered saline with Tween 20; HRP, Horseradish peroxidase; ECL, Enhanced chemiluminescence; IHC, Immunohistochemistry; DAB, 3,3'-Diaminobenzidine; ROIs, Regions of interest; AOD, Average optical density; ANOVA, Analysis of variance; SD, Standard deviation; BSA, Bovine serum albumin; HGSOC, High-grade serous ovarian cancer; EMT, Epithelial-mesenchymal transition; TLR, Toll-like receptor.

Availability of Data and Materials

The progressed scRNA sequencing data was downloaded from Gene Expression Omnibus (GEO) database including GSE184880 (GSM5599225-GSM5599231); GSE201047 (GSM6049610, GSM6049619, GSM6049625). The public TCGA-OV data used in this study are publicly available under http://xena.ucsc.edu/. The datasets used and analyzed during the current study are available from the corresponding author on reasonable request.

Author Contributions

RL: Investigation, Visualization, Writing—original draft. YF, RZ, LL, DH, LZ, QH: Investigation, Visualization. ZZ, JZ, XZ: Conceptualization, Writing—review & editing, Project administration, Funding acquisition. All contributors both read and consented to the final version of the manuscript, thereby verifying the precision of the data and findings. All authors contributed to editorial changes in the manuscript. All authors have participated sufficiently in the work and agreed to be accountable for all aspects of the work.

Ethics Approval and Consent to Participate

All experimental procedures were conducted in accordance with relevant guidelines and regulations. The study was approved by the Institutional Review Board of The Second Affiliated Hospital, Zhejiang University School of Medicine (Approval No. 2025-0642) and was conducted in accordance with the Declaration of Helsinki. Written informed consent was obtained from all participants and their legal guardians.

Acknowledgment

Not applicable.

Funding

Open access funding provided by Zhejiang University. This study was supported by the "Pioneer" and "Leading Goose" R&D Program of Zhejiang (No. 2025C02114), National Natural Science Foundation of China (No. 82203620, 32471290).

Conflicts of Interest

The authors declare no conflicts of interest.

Declaration of AI and AI-Assisted Technologies in the Writing Process

During the preparation of this work, the authors used ChatGPT only to check spelling and grammar and to improve language clarity in the Abstract, Background, Methods, Results, Discussion, Limitations, and Conclusions sections. The tool was not used to generate scientific hypotheses, design experiments, perform data analysis, create figures, or draw scientific conclusions. After using this tool, the authors carefully reviewed and edited the content as needed and take full responsibility for the content of the publication.

Supplementary Material

Supplementary material associated with this article can be found, in the online version, at https://doi.org/10.31083/FBL52801.

References

[1] Bray F, Laversanne M, Sung H, Ferlay J, Siegel RL, Soerjomataram I, et al. Global cancer statistics 2022: GLOBOCAN estimates of incidence and mortality worldwide for 36 cancers in 185 countries. CA: a Cancer Journal for Clinicians. 2024; 74: 229–263. https://doi.org/10.3322/caac.21834

[2] Lheureux S, Braunstein M, Oza AM. Epithelial ovarian cancer: Evolution of management in the era of precision medicine. CA: a Cancer Journal for Clinicians. 2019; 69: 280–304. https://doi.org/10.3322/caac.21559

[3] Batlle E, Clevers H. Cancer stem cells revisited. Nature Medicine. 2017; 23: 1124–1134. https://doi.org/10.1038/nm.4409

[4] Ahmed N, Abubaker K, Findlay JK. Ovarian cancer stem cells: Molecular concepts and relevance as therapeutic targets. Molecular Aspects of Medicine. 2014; 39: 110–125. https://doi.org/10.1016/j.mam.2013.06.002

[5] Steg AD, Bevis KS, Katre AA, Ziebarth A, Dobbin ZC, Alvarez RD, et al. Stem cell pathways contribute to clinical chemoresistance in ovarian cancer. Clinical Cancer Research: an Official Journal of the American Association for Cancer Research. 2012; 18: 869–881. https://doi.org/10.1158/1078-0432.CCR-11-2188

[6] Quail DF, Joyce JA. Microenvironmental regulation of tumor progression and metastasis. Nature Medicine. 2013; 19: 1423–1437. https://doi.org/10.1038/nm.3394

[7] Mantovani A, Marchesi F, Malesci A, Laghi L, Allavena P. Tumour-associated macrophages as treatment targets in oncology. Nature Reviews. Clinical Oncology. 2017; 14: 399–416. https://doi.org/10.1038/nrclinonc.2016.217

[8] Locati M, Curtale G, Mantovani A. Diversity, Mechanisms, and Significance of Macrophage Plasticity. Annual Review of Pathology. 2020; 15: 123–147. https://doi.org/10.1146/annurev-pathmechdis-012418-012718

[9] Qin S, Du X, Li J, Jiang N, Diao T, Bo Y, et al. Pan-cancer tumor classification by a holistic tumor microenvironment atlas. bioRxiv. 2025; 2025.12.27.696641. https://doi.org/10.64898/2025.12.27.696641 (preprint)

[10] Ma RY, Black A, Qian BZ. Macrophage diversity in cancer revisited in the era of single-cell omics. Trends in Immunology. 2022; 43: 546–563. https://doi.org/10.1016/j.it.2022.04.008

[11] Cassetta L, Pollard JW. Targeting macrophages: therapeutic approaches in cancer. Nature Reviews. Drug Discovery. 2018; 17: 887–904. https://doi.org/10.1038/nrd.2018.169

[12] Tomczak K, Czerwińska P, Wiznerowicz M. The Cancer Genome Atlas (TCGA): an immeasurable source of knowledge. Contemporary Oncology (Poznan, Poland). 2015; 19: A68–77. https://doi.org/10.5114/wo.2014.47136

[13] Xu J, Fang Y, Chen K, Li S, Tang S, Ren Y, et al. Single-Cell RNA Sequencing Reveals the Tissue Architecture in Human High-Grade Serous Ovarian Cancer. Clinical Cancer Research: an Official Journal of the American Association for Cancer Research. 2022; 28: 3590–3602. https://doi.org/10.1158/1078-0432.CCR-22-0296

[14] Loret N, Vandamme N, De Coninck J, Taminau J, De Clercq K, Blancke G, et al. Distinct Transcriptional Programs in Ascitic and Solid Cancer Cells Induce Different Responses to Chemotherapy in High-Grade Serous Ovarian Cancer. Molecular Cancer Research: MCR. 2022; 20: 1532–1547. https://doi.org/10.1158/1541-7786.MCR-21-0565

[15] Guo Y, Cui J, Liang X, Chen T, Lu C, Peng T. Pancreatic cancer stem cell-derived exosomal miR-210 mediates macrophage M2 polarization and promotes gemcitabine resistance by targeting FGFRL1. International Immunopharmacology. 2024; 127: 111407. https://doi.org/10.1016/j.intimp.2023.111407

[16] Liu M, WickremesekeraTong Z, Ding C, Luo F, Wu S, Wu C, et al. Transcription factor c-Maf is a checkpoint that programs macrophages in lung cancer. The Journal of Clinical Investigation. 2020; 130: 2081–2096. https://doi.org/10.1172/JCI131335

[17] Yang L, Shi P, Zhao G, Xu J, Peng W, Zhang J, et al. Targeting cancer stem cell pathways for cancer therapy. Signal Transduction and Targeted Therapy. 2020; 5: 8. https://doi.org/10.1038/s41392-020-0110-5

[18] Schito L, Semenza GL. Hypoxia-Inducible Factors: Master Regulators of Cancer Progression. Trends in Cancer. 2016; 2: 758–770. https://doi.org/10.1016/j.trecan.2016.10.016

[19] Tian W, Li J, Wang Z, Zhang T, Han Y, Liu Y, et al. HYD-PEP06 suppresses hepatocellular carcinoma metastasis, epithelial-mesenchymal transition and cancer stem cell-like properties by inhibiting PI3K/AKT and WNT/β-catenin signaling activation. Acta Pharmaceutica Sinica. 2021; 11: 1592–1606. https://doi.org/10.1016/j.apsb.2021.03.040

[20] Li C, Qiu S, Liu X, Guo F, Zhai J, Li Z, et al. Extracellular matrix-derived mechanical force governs breast cancer cell stemness and quiescence transition through integrin-DDR signaling. Signal Transduction and Targeted Therapy. 2023; 8: 247. https://doi.org/10.1038/s41392-023-01453-0

[21] Phi LTH, Sari IN, Yang Y-G, Lee S-H, Jun N, Kim KS, et al. Cancer Stem Cells (CSCs) in Drug Resistance and their Therapeutic Implications in Cancer Treatment. Stem Cells International. 2018; 2018: 5416923. https://doi.org/10.1155/2018/5416923

[22] Lupia M, Cavallaro U. Ovarian cancer stem cells: still an elusive entity? Molecular Cancer. 2017; 16: 64. https://doi.org/10.1186/s12943-017-0638-3

[23] You Y, Tian Z, Du Z, Wu K, Xu G, Dai M, et al. M1-like tumor-associated macrophages cascade a mesenchymal/stem-like phenotype of oral squamous cell carcinoma via the IL6/Stat3/THBS1 feedback loop. Journal of Experimental & Clinical Cancer Research. 2022; 41: 10. https://doi.org/10.1186/s13046-021-02222-z

[24] Wang S, Wang J, Chen Z, Luo J, Guo W, Sun L, et al. Targeting M2-like tumor-associated macrophages is a potential therapeutic approach to overcome antitumor drug resistance. NPJ Precision Oncology. 2024; 8: 31. https://doi.org/10.1038/s41698-024-00522-z

[25] Vento-Tormo R, Efremova M, Botting RA, Turco MY, Vento-Tormo M, Meyer KB, et al. Single-cell reconstruction of the early maternal-fetal interface in humans. Nature. 2018; 563: 347–353. https://doi.org/10.1038/s41586-018-0698-6

[26] Yang D, Sun X, Wang H, Wistuba II, Wang H, Maitra A, et al. TREM2 Depletion in Pancreatic Cancer Elicits Pathogenic Inflammation and Accelerates Tumor Progression via Enriching IL-1β^{+} Macrophages. Gastroenterology. 2025; 168: 1153–1169. https://doi.org/10.1053/j.gastro.2025.01.244

[27] Han Y, Zhang Y-Y, Pan Y-Q, Zheng X-J, Liao K, Mo H-Y, et al. IL-1β-associated NNT acetylation orchestrates iron-sulfur cluster maintenance and cancer immunotherapy resistance. Molecular Cell. 2023; 83: 1887–1902.e8. https://doi.org/10.1016/j.molcel.2023.05.011

[28] Goel HL, Mercurio AM. VEGF targets the tumour cell. Nature Reviews. Cancer. 2013; 13: 871–882. https://doi.org/10.1038/nrc3627

[29] Apte RS, Chen DS, Ferrara N. VEGF in Signaling and Disease: Beyond Discovery and Development. Cell. 2019; 176: 1248–1264. https://doi.org/10.1016/j.cell.2019.01.021

[30] Tang YH, Rockstroh A, Sokolowski KA, Lynam LR, Lehman M, Thompson EW, et al. Neuropilin-1 is over-expressed in claudin-low breast cancer and promotes tumor progression through acquisition of stem cell characteristics and RAS/MAPK pathway activation. Breast Cancer Research: BCR. 2022; 24: 8. https:

//doi.org/10.1186/s13058-022-01501-7
[31] Chen Z, Chen Y, Li Y, Lian W, Zheng K, Zhang Y, et al. Prrx1 promotes stemness and angiogenesis via activating TGF-β/smad pathway and upregulating proangiogenic factors in glioma. Cell Death & Disease. 2021; 12: 615. https://doi.org/10.1038/s41419-021-03882-7
[32] Shi X, Yang J, Deng S, Xu H, Wu D, Zeng Q, et al. TGF-β signaling in the tumor metabolic microenvironment and targeted therapies. Journal of Hematology & Oncology. 2022; 15: 135. https://doi.org/10.1186/s13045-022-01349-6
[33] Wang K, Jiang L, Hu A, Sun C, Zhou L, Huang Y, et al. Vertebral-specific activation of the CX3CL1/ICAM-1 signaling network mediates non-small-cell lung cancer spinal metastasis by engaging tumor cell-vertebral bone marrow endothelial cell interactions. Theranostics. 2021; 11: 4770–4789. https://doi.org/10.7150/thno.54235
[34] Zi R, Zhao X, Liu L, Wang Y, Zhang R, Bian Z, et al. Metabolic-Immune Suppression Mediated by the SIRT1-CX3CL1 Axis Induces Functional Enhancement of Regulatory T Cells in Colorectal Carcinoma. Advanced Science (Weinheim, Baden-Wurttemberg, Germany). 2025; 12: e2404734. https://doi.org/10.1002/advs.202404734
[35] Cheng S, Li Z, Gao R, Xing B, Gao Y, Yang Y, et al. A pan-cancer single-cell transcriptional atlas of tumor infiltrating myeloid cells. Cell. 2021; 184: 792–809.e23. https://doi.org/10.1016/j.cell.2021.01.010
[36] Fucikova J, Coosemans A, Orsulic S, Cibula D, Vergote I, Galluzzi L, et al. Immunological configuration of ovarian carcinoma: features and impact on disease outcome. Journal for Immunotherapy of Cancer. 2021; 9: e002873. https://doi.org/10.1136/jitc-2021-002873
[37] Izar B, Tirosh I, Stover EH, Wakiro I, Cuoco MS, Alter I, et al. A single-cell landscape of high-grade serous ovarian cancer. Nature Medicine. 2020; 26: 1271–1279. https://doi.org/10.1038/s41591-020-0926-0
[38] Lytle NK, Barber AG, Reya T. Stem cell fate in cancer growth, progression and therapy resistance. Nature Reviews. Cancer. 2018; 18: 669–680. https://doi.org/10.1038/s41568-018-0056-x
[39] Raghavan S, Mehta P, Xie Y, Lei YL, Mehta G. Ovarian cancer stem cells and macrophages reciprocally interact through the WNT pathway to promote pro-tumoral and malignant phenotypes in 3D engineered microenvironments. Journal for Immunotherapy of Cancer. 2019; 7: 190. https://doi.org/10.1186/s40425-019-0666-1
[40] Yin M, Li X, Tan S, Zhou HJ, Ji W, Bellone S, et al. Tumor-associated macrophages drive spheroid formation during early transcoelomic metastasis of ovarian cancer. The Journal of Clinical Investigation. 2016; 126: 4157–4173. https://doi.org/10.1172/JCI87252
[41] Murray PJ, Allen JE, Biswas SK, Fisher EA, Gilroy DW, Goerdt S, et al. Macrophage activation and polarization: nomenclature and experimental guidelines. Immunity. 2014; 41: 14–20. https://doi.org/10.1016/j.immuni.2014.06.008
[42] Xue J, Schmidt SV, Sander J, Draffehn A, Krebs W, Quester I, et al. Transcriptome-based network analysis reveals a spectrum model of human macrophage activation. Immunity. 2014; 40: 274–288. https://doi.org/10.1016/j.immuni.2014.01.006
[43] Hume DA. The Many Alternative Faces of Macrophage Activation. Front Immunol. Frontiers in Immunology. 2015; 6: 370. https://doi.org/10.3389/fimmu.2015.00370
[44] Mulder K, Patel AA, Kong WT, Piot C, Halitzki E, Dunsmore G, et al. Cross-tissue single-cell landscape of human monocytes and macrophages in health and disease. Immunity. 2021; 54: 1883–1900.e5. https://doi.org/10.1016/j.immuni.2021.07.007
[45] Zilionis R, Engblom C, Pfirschke C, Savova V, Zemmour D, Saatcioglu HD, et al. Single-Cell Transcriptomics of Human and Mouse Lung Cancers Reveals Conserved Myeloid Populations across Individuals and Species. Immunity. 2019; 50: 1317–1334.e10. https://doi.org/10.1016/j.immuni.2019.03.009
[46] Azizi E, Carr AJ, Plitas G, Cornish AE, Konopacki C, Prabhakaran S, et al. Single-Cell Map of Diverse Immune Phenotypes in the Breast Tumor Microenvironment. Cell. 2018; 174: 1293–1308.e36. https://doi.org/10.1016/j.cell.2018.05.060
[47] Bi K, He MX, Bakouny Z, Kanodia A, Napolitano S, Wu J, et al. Tumor and immune reprogramming during immunotherapy in advanced renal cell carcinoma. Cancer Cell. 2021; 39: 649–661.e5. https://doi.org/10.1016/j.ccell.2021.02.015
[48] Kawai T, Akira S. The role of pattern-recognition receptors in innate immunity: update on Toll-like receptors. Nature Immunology. 2010; 11: 373–384. https://doi.org/10.1038/ni.1863
[49] Pelka K, Hofree M, Chen JH, Sarkizova S, Pirl JD, Jorgji V, et al. Spatially organized multicellular immune hubs in human colorectal cancer. Cell. 2021; 184: 4734–4752.e20. https://doi.org/10.1016/j.cell.2021.08.003
[50] Wang W, Chen Z, Huang Y, Hu Z, Zhu P, Huang Z, et al. Integrative cross-tissue and spatially resolved single-cell profiling uncovers tumour-educated inflammatory remodelling of tissue-resident macrophage ecosystem with immunotherapeutic prognostic significance in pan-cancer. Clinical and Translational Medicine. 2026; 16: e70608. https://doi.org/10.1002/ctm2.70608
[51] Lane D, Cartier A, L'Espérance S, Côté M, Rancourt C, Piché A. Differential induction of apoptosis by tumor necrosis factor-related apoptosis-inducing ligand in human ovarian carcinoma cells. Gynecologic Oncology. 2004; 93: 594–604. https://doi.org/10.1016/j.ygyno.2004.03.029
[52] Qin T, Huang D, Liu Z, Zhang X, Jia Y, Xian CJ, et al. Tumor necrosis factor superfamily 15 promotes lymphatic metastasis via upregulation of vascular endothelial growth factor-C in a mouse model of lung cancer. Cancer Science. 2018; 109: 2469–2478. https://doi.org/10.1111/cas.13665
[53] Gama JM, Oliveira RC. CD44 and Its Role in Solid Cancers - A Review: From Tumor Progression to Prognosis and Targeted Therapy. Frontiers in Bioscience (Landmark Edition). 2025; 30: 24821. https://doi.org/10.31083/FBL24821
[54] Fakiruddin KS, Lim MN, Nordin N, Rosli R, Zakaria Z, Abdullah S. Targeting of CD133+ Cancer Stem Cells by Mesenchymal Stem Cell Expressing TRAIL Reveals a Prospective Role of Apoptotic Gene Regulation in Non-Small Cell Lung Cancer. Cancers. 2019; 11: 1261. https://doi.org/10.3390/cancers11091261
[55] Klichinsky M, Ruella M, Shestova O, Lu XM, Best A, Zeeman M, et al. Human chimeric antigen receptor macrophages for cancer immunotherapy. Nature Biotechnology. 2020; 38: 947–953. https://doi.org/10.1038/s41587-020-0462-y
[56] Prabhu VV, Morrow S, Rahman Kawakibi A, Zhou L, Ralff M, Ray J, et al. ONC201 and imipridones: Anti-cancer compounds with clinical efficacy. Neoplasia (New York, N.Y.). 2020; 22: 725–744. https://doi.org/10.1016/j.neo.2020.09.005
[57] Kline CLB, Ralff MD, Lulla AR, Wagner JM, Abbosh PH, Dicker DT, et al. Role of Dopamine Receptors in the Anticancer Activity of ONC201. Neoplasia (New York, N.Y.). 2018; 20: 80–91. https://doi.org/10.1016/j.neo.2017.10.002
[58] Hornburg M, Desbois M, Lu S, Guan Y, Lo AA, Kaufman S, et al. Single-cell dissection of cellular components and interactions shaping the tumor immune phenotypes in ovarian cancer. Cancer Cell. 2021; 39: 928–944.e6. https://doi.org/10.1016/j.ccell.2021.04.004
[59] Heath O, Berlato C, Maniati E, Lakhani A, Pegrum C, Kotantaki P, et al. Chemotherapy Induces Tumor-Associated Macrophages that Aid Adaptive Immune Responses in Ovarian Cancer. Cancer Immunology Research. 2021; 9: 665–681. https://doi.org/10.1158/2326-6066.CIR-20-0968